Dalton Transactions

PAPER

View Article Online
View Journal | View Issue

Cite this: *Dalton Trans.*, 2016, **45**, 13798

^{1}H NMR spectroscopic elucidation in solution of the kinetics and thermodynamics of spin crossover for an exceptionally robust Fe^{2+} complex†

Holm Petzold,*[a] Paul Djomgoue,[a] Gerald Hörner,[b] J. Matthäus Speck,[a] Tobias Rüffer[a] and Dieter Schaarschmidt[a]

Received 13th May 2016,
Accepted 27th July 2016

DOI: 10.1039/c6dt01895e

www.rsc.org/dalton

A series of Fe^{2+} spin crossover (SCO) complexes [Fe(**5**/**6**)]$^{2+}$ employing hexadentate ligands (**5**/**6**) with *cis*/*trans*-1,2-diamino cyclohexanes (**4**) as central building blocks were synthesised. The ligands were obtained by reductive amination of **4** with 2,2′-bipyridyl-6-carbaldehyde or 1,10-phenanthroline-2-carbaldehyde **3**. The chelating effect and the rigid structure of the ligands **5**/**6** lead to exceptionally robust Fe^{2+} and Zn^{2+} complexes conserving their structure even in coordinating solvents like dmso at high temperatures. Their solution behavior was investigated using variable temperature (VT) ^{1}H NMR spectroscopy and VT Vis spectroscopy. SCO behavior was found for all Fe^{2+} complexes in this series centred around and far above room temperature. For the first time we have demonstrated that the thermodynamics as well as kinetics for SCO can be deduced by using VT ^{1}H NMR spectroscopy. An alternative scheme using a linear correction term C^1 to model chemical shifts for Fe^{2+} SCO complexes is presented. The rate constant for the SCO of [Fe(*rac*-*trans*-**5**)]$^{2+}$ obtained by VT ^{1}H NMR was validated by Laser Flash Photolysis (LFP), with excellent agreement ($1/(k_{HL} + k_{LH})$ = 33.7/35.8 ns for NMR/LFP). The solvent dependence of the transition temperature $T_{1/2}$ and the solvatochromism of complex [Fe(*rac*-*trans*-**5**)]$^{2+}$ were ascribed to hydrogen bond formation of the secondary amine to the solvent. Enantiomerically pure complexes can be prepared starting with *R*,*R*- or *S*,*S*-1,2-diaminocyclohexane (*R*,*R*-*trans*-**4** or *S*,*S*-*trans*-**4**). The high robustness of the complexes reduces a possible ligand scrambling and allows preparation of quasiracemic crystals of [Zn(*R*,*R*-**5**)][Fe(*S*,*S*-**5**)]$(ClO_4)_4 \cdot (CH_3CN)$ composed of a 1 : 1 mixture of the Zn and Fe complexes with inverse chirality.

Introduction

Octahedral complexes of Fe^{2+} can exist in two different spin states: the paramagnetic high spin (HS) state (S = 2) or the diamagnetic low spin (LS) state (S = 0). In a nitrogen-dominated ligand environment, both spin states are often close in energy and a temperature-dependent equilibrium is found. The molar ratio between the HS state and the LS state can be addressed by external stimuli like irradiation with light, heating or cooling. Such spin crossover (SCO) complexes have been discussed for many applications in, for example, data storage devices or as switches in electronics.[1–6] Apart from such sophisticated applications, applications such as thermochromics or in functional magnetic resonance tomography (MRT) can be envisioned.

One requirement in this regard is robustness and stability against oxidation and hydrolysis. In particular, the HS Fe^{2+} complexes are often lacking in robustness due to the small ligand field stabilisation energy. Chelating ligands can help to stabilise HS Fe^{2+} complexes kinetically as well as thermodynamically.

In this regard, we have recently introduced Fe^{2+} SCO complexes employing a hexadentate ligand that can be obtained by condensation of 2,2′-diaminobiphenyles and [2,2′-bipyridine]-6-carbaldehyde or 6′-substituted derivatives.[7–9] The complexes are stable against hydrolysis in water, but strongly coordinating solvents like dmso replace the hexadentate ligands. We also found that the presence of aminomethylene units directly bound to the aromatic ring increases the sensitivity towards oxidation[9,10] leading to imines as well as amides. *N*-Methylation shuts down this sensitivity but, at the same time, shifts the HS/LS equilibrium completely to the HS state side.[9]

[a]*TU Chemnitz, Institut für Chemie, Anorganische Chemie, Straße der Nationen 62, 09111 Chemnitz, Germany. E-mail: holm.petzold@chemie.tu-chemnitz.de; Fax: +49-371-53137463*
[b]*TU Berlin, Institut für Chemie, Straße des 17. Juni 135, 10623 Berlin, Germany*

†Electronic supplementary information (ESI) available. CCDC 1472618–1472622. For ESI and crystallographic data in CIF or other electronic format see DOI: 10.1039/c6dt01895e

To circumvent this problem, the 2,2′-diaminobiphenyl bridge can be replaced by aliphatic diamines, *e.g.*, 1,2-diaminocyclohexanes (**4**). Complexes of this type were reported before by Constable,[11] Kol[12] and Blackman.[13,14] However, all of those Fe^{2+}-complexes were described as LS Fe^{2+} complexes. Herein, we wish to report topologically related complexes that employ an aliphatic 1,2-diaminocyclohexane (**4**) fragment as the bridge. These complexes show SCO at elevated temperatures and are exceptionally robust. In addition the rigid structure and robustness of the complexes allow an in-depth survey of the ^{1}H-NMR spectroscopic properties. NMR spectroscopy is one of the most versatile methods to investigate compounds and reactions in solution.[15] Here we use this opportunity to present a consistent and general model for the interpretation of ^{1}H NMR spectra of Fe^{2+} spin crossover complexes in solution. Moreover we will demonstrate that both thermodynamics as well as kinetics of the SCO can be conveniently derived from VT ^{1}H-NMR spectra (VT = variable temperature).

Results and discussion

Synthesis of ligands 5 and 6 and their Fe^{2+} complexes

1,10-Phenanthroline-2-aldehyde **3** was prepared following a protocol from Pallavicini *et al.*[16] Starting from 1,10-phenanthroline **1**, methylation[17] yields compound **2**. By oxidation of **2** with SeO_2, aldehyde **3** was obtained.[16] The ligands **5** were obtained by condensation of 1,10-phenanthroline-2-carbaldehyde **3** with cyclohexane-1,2-diamine **4**, followed by reduction with sodium borohydride (Scheme 1). Additional treatment of *rac-trans*-**5** with formaldehyde and sodium borohydride[18] allowed the methylation of the secondary amine group to obtain *rac-trans*-NMe-**5**. Compounds **5** are in general air sensitive viscous oils.

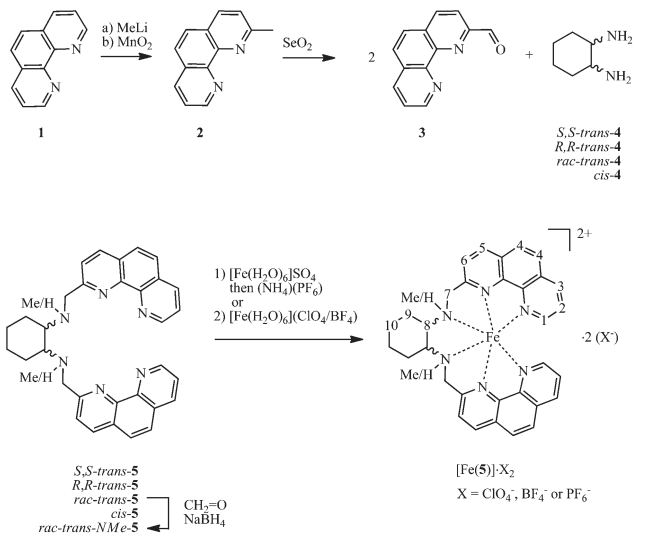

Scheme 1 Syntheses of the ligands **5** and their reaction with Fe^{2+} yielding compounds $[Fe(\mathbf{5})]^{2+}X_2$. The numbers in italics show the position labels as used for subsequent discussion of NMR spectra. The two chemically different CH_2-protons in positions 7, 9, and 10 were referred to H(7, 9 or 10)-1 and H(7, 9 or 10)-2.

Treatment of ligands **5** with $[Fe(OH_2)_6]SO_4$ and subsequent anion exchange, or using the appropriate Fe^{2+} salts, in ethanol or acetonitrile solutions instantly results in the formation of deep purple solutions. The corresponding compounds with the general formula $[Fe(\mathbf{5})]X_2$ precipitate from ethanol solution. The complex salts $[Fe(\mathbf{5})]X_2$ with X = BF_4^- or ClO_4^- are well soluble in aprotic, polar organic solvents like acetonitrile (acn), dimethylformamide (dmf), dimethyl sulfoxide (dmso) or acetone. They are sparingly soluble in dichloromethane, ethanol and insoluble in diethyl ether. Exchange of the counter ion with bromide leads to water soluble compounds. Similarly, the analogous bipyridine-based complex [Fe(*rac-trans*-NMe-**6**)]$(BF_4)_2$ was obtained (Scheme 2).

The compounds revealed reasonable elemental analysis data and mass spectra in agreement with mononuclear complexes and a ligand to metal ratio of 1 : 1. It is noted that the NMR spectra of crude [Fe(*rac-trans*-**5**)$_2$]$(BF_4)_2$ showed small additional signals which were assigned to a dinuclear complex. Similar observations were reported by Constable *et al.* for a related system.[11] Materials of significantly higher purity are obtained by recrystallisation from acn/isopropanol. The proton NMR spectra of [Fe(*rac-trans*-**5**)$_2$]$(BF_4)_2$ show typical features of SCO Fe^{2+} complexes, such as significantly shifted resonances and broad lines. Nevertheless, the expected number of signals requested for a C_2 symmetric complex was found in the range of 0.7 to 20 ppm. Proton NMR spectra of the *cis*-analog [Fe(*cis*-**5**)$_2$]$(BF_4)_2$ are more complicated, likely due to molecular dynamics (*vide infra*).

NMR analysis of spin crossover

SCO thermodynamics. The colour of complexes $[Fe(\mathbf{5})]^{2+}$ reversibly changes from deep purple to red on raising the temperature in high boiling solvents like propylene carbonate, dmf or dmso. This thermochromic behavior is the optical manifestation of a thermal equilibrium between the HS and LS states of the complexes. Indeed, both the positions and widths of the resonance lines in the proton NMR spectra of the Fe^{2+} complexes were generally temperature dependent. Besides this, we noticed that the chemical shifts in the spectra of [Fe(*rac-trans*-**5**)]$(BF_4)_2$ are solvent dependent, whereas this effect was less pronounced in the case of *N*-methylated [Fe(*rac-trans*-NMe-**5**)]$^{2+}$. In order to gain more insight into the solvent and temperature dependence, the complexes [Fe(*rac-trans*-**5**)]$^{2+}$ and [Fe(*rac-trans*-NMe-**5**)]$^{2+}$ were thoroughly investigated by variable-temperature proton NMR spectroscopy (VT ^{1}H NMR) (Fig. 1). In the text below we focus on the results of this investigation and provide only a brief description of the methods employed. A more detailed description and validation of the methods is given in the ESI† to this paper.

Assignment of the signals to the protons was based on ^1H,^1H-COSY spectroscopy at low temperature, supplemented by T_1 times recorded at room temperature (see below). The assignment of the protons in the HS form of the complexes

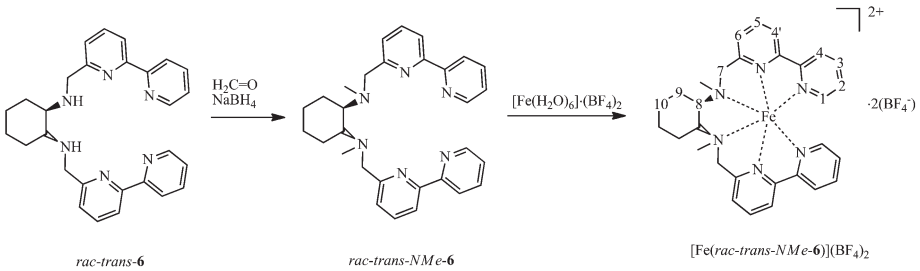

Scheme 2 Syntheses of the *N*-methylated ligand *rac-trans*-NMe-**6** and of compound [Fe(*rac-trans*-NMe-**6**)]$(BF_4)_2$. For synthesis and properties of [Fe(*rac-trans*-**6**)]$(BF_4)_2$, see ref. 11. The numbers in italics give the numbering scheme for discussions on proton NMR spectroscopy. Note that the protons in positions 4/4′ were not unambiguously assigned and therefore treated together. The two chemically different CH_2-protons in positions 7, 9, and 10 are referred to as H(7, 9 or 10)-1 and H(7, 9 or 10)-2.

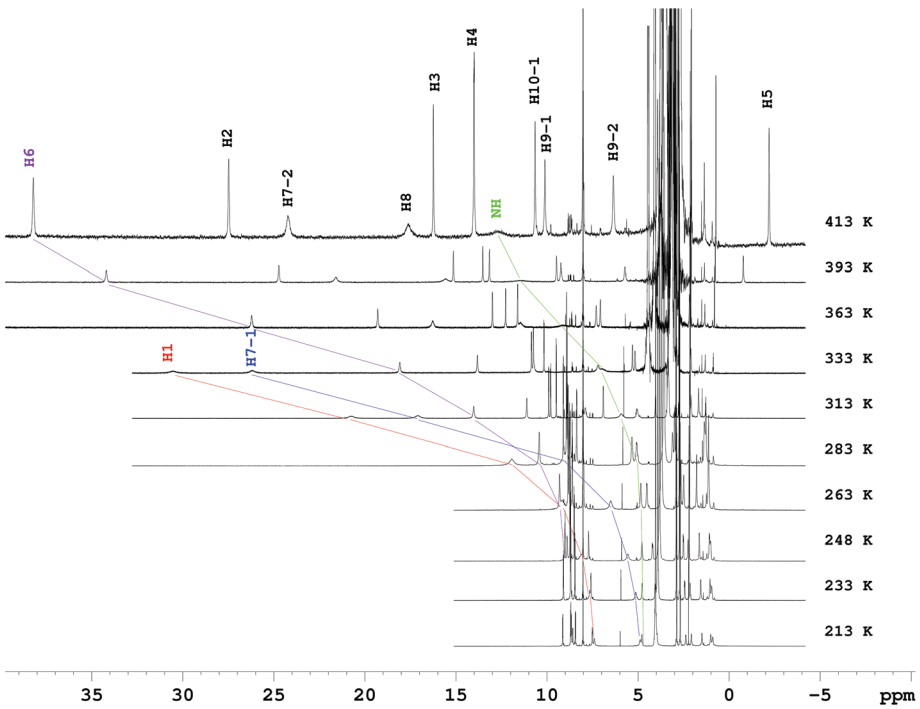

Fig. 1 VT ^{1}H NMR spectra of complex [Fe(*rac-trans*-**5**)]$^{2+}$ in d_7-dmf-solution. The given temperatures are target temperatures of the probe.

relies on tracking of the resonances during the transition from the LS to the HS state; a method which benefits from the high transition temperature $T_{\frac{1}{2}}$. In cases where this is not possible, we found the analysis of the longitudinal relaxation times ($T_1 \propto 1/r^6$) advantageous, when combined with a proper molecular model. By correlating the paramagnetic contribution to the chemical shift or the linewidths (transversal relaxation time T_2) with the H⋯Fe distance, only a rough qualitative picture for the assignment of the proton sites can be obtained. In particular, the chemical shifts are a sum of different contributions (with positive and negative signs) from different coupling mechanisms[19] and the linewidths in the spectra of Fe^{2+} SCO complexes are often dominated by exchange broadening (*vide infra*).

In order to extract the transition temperature $T_{\frac{1}{2}}$ and the thermodynamic parameters $\Delta_{SCO}H$ and $\Delta_{SCO}S$ of the HS/LS equilibrium, the observed chemical shifts $\delta_{obs}(T)$ were analysed. Generally, HS/LS equilibration for Fe^{2+} SCO complexes is rapid with respect to the NMR time scale, so that the chemical shifts are the average of the chemical shifts $\delta_{HS}(T)$ and δ_{LS} of the molecules in the LS and HS states, respectively, weighted by the HS and LS fraction (eqn (1) and (2)). While in eqn (1)–(3), δ_{LS} can be treated as temperature independent, the chemical shift of the HS state $\delta_{HS}(T)$ is intrinsically temperature dependent.[20,21] In a first order approximation, the temperature dependence of the chemical shifts in paramagnetic complexes can be calculated using a Curie-like model with a Curie constant $C_i(T)$ for a particular proton site i:[20,22] $\delta_{HS}(T) = C_i(T)/T +$

$(\delta_{dia})_i$. $(\delta_{dia})_i$ are the diamagnetic contributions to the chemical shifts of the HS state.

$$\delta_{obs}(T) = \gamma_{HS}(T)\delta_{HS}(T) + \gamma_{LS}(T)\delta_{LS} \quad (1)$$

$$\delta_{obs}(T) = \gamma_{HS}(T)\delta_{HS}(T) + (1 - \gamma_{HS}(T))\delta_{LS} \quad (2)$$

$$\gamma_{HS}(T) = \frac{\delta_{obs}(T) - \delta_{LS}}{\delta_{HS}(T) - \delta_{LS}} = \frac{1}{\left(1 + e^{\left(\frac{\Delta_{SCO}H}{R}\left(\frac{1}{T} - \frac{\Delta_{SCO}S}{\Delta_{SCO}H}\right)\right)}\right)} \quad (3)$$

$$\delta_{HS}(T) = \left(\delta_{dia} + \frac{C(T)}{T}\right) \quad (4)$$

$$\gamma_{HS}(T) = \frac{\left(\delta_{obs}(T) - \delta_{LS/dia}\right)T}{C(T)} \quad (5)$$

$$\gamma_{HS}(T)C(T) = \left(\delta_{obs}(T) - \delta_{LS/dia}\right)T = \frac{C(T)}{\left(1 + e^{\left(\frac{\Delta_{SCO}H}{R}\left(\frac{1}{T} - \frac{\Delta_{SCO}S}{\Delta_{SCO}H}\right)\right)}\right)} \quad (6)$$

'Classical refinement' with temperature-invariant Curie constants. In most cases studied here, the Curie constants $C_i(T)$ could be satisfyingly treated as temperature independent; that is, $C_i(T) = C_i^0$; in the following, this method is named 'classical refinement'. In addition, δ_{LS} and δ_{dia} were set equal, subsumed in $\delta_{dia/LS}$ (justification is given in the ESI†). With this approach, reasonable results had been obtained by others for $\Delta_{SCO}H$ and $\Delta_{SCO}S$ in related complexes.[22,23] In our work, the 'classical refinement' was used to calculate $\Delta_{SCO}H$ and $\Delta_{SCO}S$ for complex $[Fe(rac\text{-}trans\text{-}\mathbf{5})]^{2+}$ in d_5-pyridine, d_7-dmf and d_5-nitrobenzene solution, using the six proton sites with the strongest temperature dependence (H1, H7-1, H6, H2, NH, H7-2, H5) (Table 1 gives a summary, details are reported in ESI Tables 3-SI and 4-SI†).

In order to allow for fitting to a sigmoidal curve, the product of the HS-fraction and Curie constant was calculated using eqn (6) and (5). Reasonable values for $\delta_{dia/LS}$ were approximated from spectra recorded at the lowest temperatures accessible. For d_5-nitrobenzene with its high melting point, $\delta_{dia/LS}$ values were approximated by data from d_7-dmf solution.

It is found that the freely refined Curie constants $C_i(T)$ differ less than ±10% in different solvents. With the exception of H5, positive Curie constants were found for all protons (for a possible explanation see the ESI†). The two protons H1 and H7-1 with the largest temperature dependence in the chemical shifts yield Curie constants in the range of 47 000 and 42 000 ppm K. The protons at the *meta* position, with respect to the phenanthroline nitrogen atoms, show smaller Curie constants of about 13 000 and 20 000 ppm K. The NH proton, which is closest to the Fe atom, shows a considerably smaller Curie constant of about 7000 ppm K. These latter results for the nitrogen-bound protons (NH-proton) were rejected as outliers and are only given for completeness.

An apparently proton-site inherent variance in such-derived transition temperatures $T_{\frac{1}{2}}$ of 6.5 K and 5.0 K in d_5-pyridine and d_5-nitrobenzene, respectively, points to unaccounted secondary temperature effects. Accordingly, more satisfying inner consistency of the transition temperatures was achieved by accounting for the temperature dependence of the Curie constants with 1st-order corrections in T (*vide infra*). Nevertheless, irrespective of the uncertainties inherent in the classical refinement, $[Fe(rac\text{-}trans\text{-}\mathbf{5})]^{2+}$ clearly exhibits solvent-dependent SCO; *i.e.*, the solvent-invoked variance in the transition temperatures ($\Delta T_{1/2}$(solv) ≈ 50 K) significantly exceeds the site-inherent variance ($\Delta T_{1/2}$(site) ≈ 5 K). This finding of a significant solvent effect on the thermodynamics of SCO is of relevance, as only a few examples for solvent-dependent spin crossover have been previously described in the literature. An eminent example was published by Halcrow *et al.*, who

Table 1 NMR-derived thermodynamic data for SCO of complex $[Fe^{2+}(rac\text{-}trans\text{-}\mathbf{5})]^{2+}$. Data are the average of parameters for proton sites H1, H2; H5; H6; H7-1 and H7-2; for comparison, UV-Vis derived data are also given. Standard deviations for single site refinements are given in the ESI in Tables 3-SI and 4-SI

Solvent ($[Fe(rac\text{-}trans\text{-}\mathbf{5})]^{2+}$)	$\Delta_{SCO}H$ (kJ mol^{-1})	$\Delta_{SCO}S$ (J mol^{-1} K^{-1})	$T_{\frac{1}{2}}$ (K)	max $T_{\frac{1}{2}}$ (K)	min $T_{\frac{1}{2}}$ (K)
NMR: full classical refinement					
d_5-Pyridine	30.4	80	381	383.1(±3.9); H7-1	377.4(±4.8); H6
d_7-dmf	30.9	78.7	393	396.8(±0.8); H2	390.6(±2.1); H5
d_5-nitrobenzene	28.1	79.2	355	357.1(±0.3); H6	352.1(±2.1); H5
NMR: parameterised classical refinement[a]					
D_2O	33.7	82.9	406		
d_6-dmso	30.8	76.6	403		
d_3-acn	30.8	81.7	377		
VT vis spectroscopy[b]					
dmf	33.4(0.1)	85.5	390.6(0.2)		
nitrobenzene	28.1(0.2)	78.3	358.4(0.2)		
In epoxy resin	30.2(0.2)	79.4	380.2(0.2)		

[a] Curie constants C^0 were set to fixed values, calculated from data of experiments in d_7-dmf, d_5-nitrobenzene and d_5-pyridine solution. [b] Details for the data processing are reported in the ESI.

associated a variance in $T_{\frac{1}{2}}$ of 100 K in water and acetone solution with effects of H-bonding of ligand-appended protic NH groups;[24] similar findings had been reported by Linert *et al.* for complexes with NH-containing benzimidazole ligands,[25] corroborating the notion of the cyclohexylamine-borne NH groups harboring the solvent dependence in the present case of [Fe(*rac-trans*-**5**)]$^{2+}$. Related supramolecular effects on the SCO transition temperatures followed from variation of the counterion in nonpolar solvents were reported by Shores.[26–28] In agreement with this conclusion, the SCO of the *N*-methylated congener [Fe(*rac-trans*-NMe-**5**)]$^{2+}$ is found far less susceptible towards solvent effects (*vide infra*). It is noted that hydrogen bonds are actively influencing SCO in the solid state also and that they hold importance for the occurrence of hysteresis loops in solid samples.[29–31]

Parameterised 'classical refinement' with temperature-invariant Curie constants. In order to put our methodological approach on a broader experimental basis, additional temperature dependent ^{1}H NMR spectra were recorded in d_3-acn, d_6-dmso and D_2O solution. In order to solubilise [Fe(*rac-trans*-**5**)](X)$_2$ also in aqueous media, it was extracted from a CH_2Cl_2/d_3-acn solution with D_2O in the presence of (N^nBu_4)(Br).

All three solvents have limitations in the temperature range applicable to solution NMR spectroscopy. This impedes a free refinement of C^0; attempts reveal over-parameterisation and unstable refinement. In order to stabilise the refinement and to avoid over-parameterisation, NMR-parameters representing the HS and LS state had to be approximated.

(i) The chemical shifts of proton sites in HS-[Fe(*rac-trans*-**5**)]$^{2+}$ were approximated with fixed Curie constants, C_i. The latter were extracted from previous measurements by averaging the Curie constants in d_7-dmf, d_5-pyridine and d_5-nitrobenzene solution for each particular proton site.

(ii) As an approximation of the chemical shifts of protons in LS [Fe^{2+}(*rac-trans*-**5**)]$^{2+}$, $\delta_{dia/LS}$ values from d_7-dmf solution at low temperature were used.

With these approximations in hand, reasonable fits were obtained (an example for acn solution is given in the ESI, Fig. 9-SI and 10-SI†). The transition temperatures $T_{\frac{1}{2}}$ were calculated as 377 K, 403 K and 406 K in d_3-acn, d_6-dmso and D_2O solution, respectively (Table 1). These results corroborate our previous notion of a highly solvent-susceptible SCO in [Fe^{2+}(*rac-trans*-**5**)]$^{2+}$. The second important conclusion to be drawn from these findings is that the compound is exceptionally robust against solvolysis, exposure to moisture, and oxidation in air under harsh conditions, even at elevated temperatures and even in strongly coordinating solvents. The excellent fits with reasonably small ranges of $\Delta_{SCO}S$, the complete reversibility of the phenomena, and the small linewidths at higher temperature are all indicative of the high robustness of the complex. That is, even in the presence of air in dmso solution, NMR spectra could be recorded up to the highest temperature only limited by probe head specifications.

According to our previous results, *N*-methylation should prevent a degradation of the aminomethylene linker by oxidation. Indeed the *N*-methylated counterpart [Fe(*rac-trans*-NMe-**5**)]$^{2+}$ is similarly robust. Initial inspection of the temperature dependent ^{1}H NMR spectra clearly revealed a spin equilibrium in [Fe(*rac-trans*-NMe-**5**)]$^{2+}$, compared to the non-methylated congener [Fe(*rac-trans*-**5**)]$^{2+}$, with a higher transition temperature $T_{\frac{1}{2}}$. The transition temperatures were calculated by refinement of the observed chemical shifts. Due to the fact that $T_{\frac{1}{2}}$ is higher than the highest temperature available for solution ^{1}H NMR spectroscopy, a stable refinement with freely refined Curie constants is not possible. Therefore, fixed Curie constants had to be used, as outlined above for [Fe^{2+}(*rac-trans*-**5**)]$^{2+}$ in the parameterised refinement. As the respective data are not genuinely accessible for [Fe(*rac-trans*-NMe-**5**)]$^{2+}$, we decided to use fixed Curie constants, derived from d_7-dmf, d_5-pyridine and d_5-nitrobenzene solutions of [Fe^{2+}(*rac-trans*-**5**)]$^{2+}$. This data transfer appears justified, because inspection of these spectra revealed an obvious qualitative similarity (direction and magnitude of paramagnetic induced shifts of the resonances) of the NMR spectra and the temperature dependent shifts of [Fe(*rac-trans*-NMe-**5**)]$^{2+}$ and [Fe(*rac-trans*-**5**)]$^{2+}$. It turned out that only for the proton site H7-2 the Curie constants differ notably between the methylated and non-methylated complex. This singularity can be safely assigned to the influence of the additional methyl group (*vide infra*). Reasonable results of refinement are obtained this way (summary in Table 2, details are in the ESI†), further supporting the validity of the chosen approach.

In order to validate the results obtained from NMR analysis, we conducted variable temperature Vis-spectroscopy on complex [Fe(*rac-trans*-**5**)]$^{2+}$ in dmf and nitrobenzene solution. The intense MLCT bands between 450 nm and 650 nm are typical of the LS spin state, whereas the HS state absorbs at considerably shorter wavelengths. This allows following the spin crossover by using the absorption at 564 nm. Within experimental errors, the results of the VT Vis spectroscopy and the NMR refinements are consistent (Table 1).

The solution studies, especially in the coordinating solvents like dmso, acetic acid/acn and dmf, were only possible due to the exceptional robustness of the complexes. Robust materials are a prerequisite for many applications. To further demonstrate the inertness of complexes [Fe(*rac-trans*-**5**)]$^{2+}$ and

Table 2 Thermodynamic data for complex [Fe(*rac-trans*-NMe-**5**)]$^{2+}$. Data were obtained by fitting to the HS fraction calculated from sites H1, H2; H5; H6; H7-1. For details see the ESI

[Fe^{2+}(*rac-trans*-NMe-**5**)]$^{2+}$ solution by NMR	$\Delta_{SCO}H$ (kJ mol^{-1})	$\Delta_{SCO}S$ (J mol^{-1} K^{-1})	$T_{\frac{1}{2}}$ (K)
d_3-acn/d_4-acetic acid (2.5 : 4)	32.4	74.8	433
d_6-dmso	32.5	73.6	442
d_3-acn	33.9	79.3	427
d_5-nitrobenzene	33.1	76.5	432
VT UV/Vis[a] [Fe^{2+}(*rac-trans*-NMe-**5**)]$^{2+}$ in epoxy resin	25.8(0.2)	62.9	411.4(0.5)
[Fe(*cis*-**5**)]$^{2+}$ acetone solution	20.1(0.1)	72.7	276.2(0.1)

[a] Details for the data processing are reported in the ESI.

$[Fe(rac\text{-}trans\text{-}NMe\text{-}\mathbf{5})]^{2+}$, we embedded their hexafluorophosphate salts into an epoxy resin. By simply dissolving the compounds in the hardener and mixing it with the binder we could obtain thermochromic materials. Though the compounds are only sparingly soluble in the hardener, the resulting concentrations (<1 mM) were sufficient to record reversible thermochromic cycles upon heating and cooling. The results from quantitative analyses of the temperature dependent absorption changes at λ = 565 nm agree well with those of the solution studies and confirm SCO to be the molecular origin of the thermochromic effect. It should be noted that the dication $[Fe(cis\text{-}\mathbf{5})]^{2+}$ decomposes during mixing with the hardener and that $[Fe(rac\text{-}trans\text{-}\mathbf{5})]^{2+}$ is vulnerable at higher temperature (>400 K) in the presence of oxygen. In contrast, the methylated complex $[Fe(rac\text{-}trans\text{-}NMe\text{-}\mathbf{5})]^{2+}$ is very robust even in the presence of air.

The derived transition temperatures of $[Fe(rac\text{-}trans\text{-}NMe\text{-}\mathbf{5})]^{2+}$ fall in a narrow range (427 K < $T_{1/2}$ < 442 K) with the minimum and maximum values observed in acn and dmso solution, respectively (Table 2). The entropy changes $\Delta_{SCO}S$ range from 73.6 J mol^{-1} K^{-1} to 79.3 J mol^{-1} K^{-1}. Given the uncertainties due to the high transition temperatures, the solvent dependence of the spin equilibrium of $[Fe(rac\text{-}trans\text{-}NMe\text{-}\mathbf{5})]^{2+}$, if any, is not discussed in greater detail. Nevertheless, the transition temperatures of $[Fe(rac\text{-}trans\text{-}NMe\text{-}\mathbf{5})]^{2+}$ are certainly substantially less prone to solvent effects than $[Fe(rac\text{-}trans\text{-}\mathbf{5})]^{2+}$.

The room temperature ^{1}H-NMR spectra for complex $[Fe(rac\text{-}trans\text{-}NMe\text{-}\mathbf{6})]^{2+}$ show well resolved resonances, typical of a well-defined LS-Fe^{2+}-complex. Not unexpectedly, however, the ^{1}H NMR spectra recorded in d_5-nitrobenzene in the temperature range 283 K–403 K (see Fig. 14-SI†), reveal a temperature dependence of the chemical shifts that is akin to $[Fe(rac\text{-}trans\text{-}NMe\text{-}\mathbf{5})]^{2+}$ and $[Fe(rac\text{-}trans\text{-}\mathbf{5})]^{2+}$. However, from these data it is also obvious that the HS fraction of the former complex, even at the highest temperature, is much less than 10% (Fig. 14-SI†). A further reduction in parameters is thus necessary for refinement. An inspection of the entropy data collected in Tables 1 and 2 reveals this parameter to be only weakly susceptible to structure effects, $\Delta_{SCO}S$ was fixed at 80 J mol^{-1} K^{-1}. Using a similar treatment as described before (but with fixed $\Delta_{SCO}S$ and Curie constants from d_7-dmf solution), the data yielded a reasonable fit for a transition temperature of 570 K. Again obvious deviations are found for the proton H7-2 that is affected by the methyl group.

Attempts to determine the thermodynamic data of the *cis*-analog complex $[Fe(cis\text{-}\mathbf{5})]^{2+}$ by ^{1}H NMR spectroscopy were unsuccessful, due to atypical behavior (spectra are given in the ESI Fig. 23-SI†). Complementary data obtained by VT Vis spectroscopy indicate an early SCO, being centered at $T_{\frac{1}{2}}$ = 276 K and $\Delta_{SCO}S$ = 72.7 J mol^{-1} K^{-1} (Table 2). The huge effect of stereochemistry of the diamine bridge **4** on the SCO thermodynamics is mainly ascribable to enthalpic effects due to the similarity of $\Delta_{SCO}S$ = 72.7 J mol^{-1} K^{-1} with the *trans*-analog complexes. However the principal NMR features, such as decreased paramagnetic shifts at low temperature and the appearance of a new set of broad signals in the typical diamagnetic region (11 ppm to 0 ppm) at 183 K reflect the spin transition deduced from VT Vis spectroscopy. We are not yet able to unambiguously explain these extraordinary broadenings of the NMR resonance lines. Likely additional intramolecular dynamics cause the additional line broadening which hampers analysis of the NMR data; preferential conformations of the cyclohexyl ring are suspected to vary with the spin state.

Improved refinement with 1st-order temperature-dependent Curie constants. It should be noted here that chemical shifts have been measured for complex $[Fe(rac\text{-}trans\text{-}\mathbf{5})]^{2+}$ in a temperature range that spans more than 200 K (210 K to 417 K). Although the agreement between calculated and observed chemical shifts was fairly good ($(\delta_{obs} - \delta_{calcd})$ < 0.3 ppm and $\Delta\gamma_{HS}(T)$ < 0.2% see Fig. 5-SI and 8-SI in the ESI†) over the entire temperature range, still there was room and need for improvement. In particular, a look at the confidence intervals calculated for $T_{\frac{1}{2}}$ revealed a significant variation in the transition temperatures $T_{\frac{1}{2}}$ calculated by using different proton sites for d_5-pyridine and d_5-nitrobenzene as well as d_7-dmf. In other words, from the statistical point of view, the transition temperatures differ significantly with the chosen proton site. This variation is not acceptable, as a refinement using a particular proton site of a given complex must give identical transition temperatures for a particular solvent regardless of the proton site used. This finding points to a small biased error, which we associate with an uncompensated temperature dependence of the Curie constants. Indeed, it has been shown before that both in practice and theory, C_i are temperature dependent.[20,32–34] Reasonable schemes taking into account zero field splitting, low lying excited states as well as molecular dynamics have been presented.[20,32,33]

In the case of Fe^{2+} complexes, the temperature dependence of $C(T)$ is caused by the successive population of low lying excited states and by zero field splitting.[32,35,36] A full treatment of all of these effects in solution NMR spectroscopy is difficult, even in the absence of SCO,[33,34] and requires exceptionally accurate NMR data. As a minor point, δ_{dia} is not exactly equal to δ_{LS} (see Table 2-SI†). In order to account for the temperature dependence of $C(T)$, we decided to follow suggestions from the literature[33,37] and applied a linear correction by the introduction of C^1 (eqn (7)). The validity of this approach is discussed in detail in the ESI.† As $C(T)$ is given in units of K ppm, C^1 must have the dimension of a chemical shift and is given in units of ppm.

$$C(T) = C^0 + C^1 T \tag{7}$$

$$\delta_{obs}(T) = \gamma_{HS}(T)\left(\delta_{dia} + \frac{C^0}{T} + C^1\right) + (1 - \gamma_{HS}(T))\delta_{LS} \tag{8}$$

$$\delta_{obs}(T) = \gamma_{HS}(T)\left(\frac{C^0}{T} + C^{1*}\right) + \delta_{LS} \tag{9}$$

$$C^{1*} = C^1 + \delta_{dia} - \delta_{LS} \tag{10}$$

As a positive side effect, the new parameter C^1 corrects also the difference between δ_{dia} and δ_{LS}. However, the effects on the results is small and in the following discussion we do not differ-

entiate between C^1 and C^{1*} and rename δ_{LS} as $\delta_{dia/LS}$. In this improved refinement, for every proton site three proton specific parameters, C^0, C^1, and $\delta_{dia/LS}$, need to be refined. A homemade Excel script allowed us to refine only a single global $\Delta_{SCO}H$ as well as a single $\Delta_{SCO}S$ for all proton sites of a complex together. Necessarily, this approach yields only a single transition temperature irrespective of the number of proton sites used.

To demonstrate the efficiency of this correction, the refinement of ^{1}H NMR data for complex $[Fe^{2+}(rac\text{-}trans\text{-}5)]^{2+}$ in d_7-dmf, d_5-pyridine and d_5-nitrobenzene solution was repeated. The global values for $\Delta_{SCO}H$ as well as $\Delta_{SCO}S$ were set at the averaged values found for a particular solvent in the classical refinement. The proton site specific parameters, C^0, C^1, and $\delta_{dia/LS}$, were refined freely. Very accurate fits were obtained (Fig. 2 and 7-SI†) with very small differences between the calculated and observed chemical shifts (<0.15 ppm) for all resonances at all temperatures and a single $\Delta_{SCO}H$ and single $\Delta_{SCO}S$ for all proton sites. This demonstrates that the temperature dependence of $C(T)$ is indeed responsible for disagreements in the classical refinement and linear correction with C^1 is sufficient to obtain full agreement of calculated and experimentally obtained shifts (Fig. 2). However, we also found that introduction of the parameter C^1 also increases the degree of freedom drastically. That is, very accurate fits of the experimental data are obtained at the expense of a wider range of values of $\Delta_{SCO}H$, $\Delta_{SCO}S$ and proton specific NMR parameters, again indicating over-parameterisation.

To sum up the NMR approach to the thermodynamics, the correction for the temperature dependency of the Curie constant $C(T)$ according to eqn (7) can be fruitful but only for exceptionally exact data, recorded in large temperature ranges covering temperatures below and considerably above $T_{\frac{1}{2}}$. For refinements where the HS fraction remains considerably above 5% at the lowest accessible temperatures due to the high melting point of the solvent, $\delta_{dia/LS}$ parameters should be fixed at reasonable values. In many cases classical refinement is sufficient. With well-chosen approximations for $\delta_{dia/LS}$ and/or C^0, transition temperatures far above the experimentally available temperature range can be estimated.

SCO kinetics. With the detailed knowledge of the chemical shifts and the thermodynamic parameters $\Delta_{SCO}H$ and $\Delta_{SCO}S$ in hand, the kinetic parameters for SCO, *e.g.* forward and backward reaction rate constants, k_{HL} and k_{LH}, can be extracted from the NMR spectra. To the best of our knowledge, this was never demonstrated before for Fe^{2+} spin crossover complexes solely based on ^{1}H-NMR data (a detailed description of the methods used is given in the ESI†). We became aware of this possibility by a closer look at the linewidths found in the ^{1}H NMR spectra (Fig. 4).

A brief description of proton relaxation

Proton spin relaxation in HS-Fe^{2+} complexes is mainly caused by the dipolar coupling between the proton spin and the spin of the fast relaxing electrons. Hence, the relaxation rates are dependent on the distance of the proton to the metal, the electron relaxation rate ($R_s = 1/\tau_s$ for dipolar relaxation), and the rotational correlation time (τ_r for Curie relaxation). Solomon–Bloembergen equations (see the ESI†) predict for the proton relaxation rates[20] a constant ratio between longitudinal and transversal relaxation (R_1 and R_2, respectively). For proton relaxation rates, the relationship $R_2 > R_1$ must hold. With increasing electron relaxation rates R_s and faster rotation this should approach unity. For octahedral Fe^{2+} complexes, fast electron relaxation ($\tau_s = 10^{-12}$ s to 10^{-13} s)[20] is expected. The rotational correlation times τ_r can be calculated by the Einstein equation using the diameter of the complex and the viscosity of the solvent.

Often the assignments of protons of paramagnetic complexes are based on the relationship of the relaxation times T_n (LW frequently named $\Delta\nu_{\frac{1}{2}}$) to the metal–proton distance r ($1/T_n \propto 1/r^6$). While the longitudinal relaxation rates ($R_1 = 1/T_1$) recorded for $[Fe^{2+}(rac\text{-}trans\text{-}5)]^{2+}$ obey this rule perfectly (Fig. 3), the relaxation times ($\pi LW = R_2 = 1/T_2$) recorded around room temperature are not consistent with this rule (see Fig. 4). That is, the relaxation times and, consequently, the linewidths are obviously convoluted with an additional component of dynamics.

The difference between expected and experimental results found for the linewidths can be ascribed to dynamic exchange

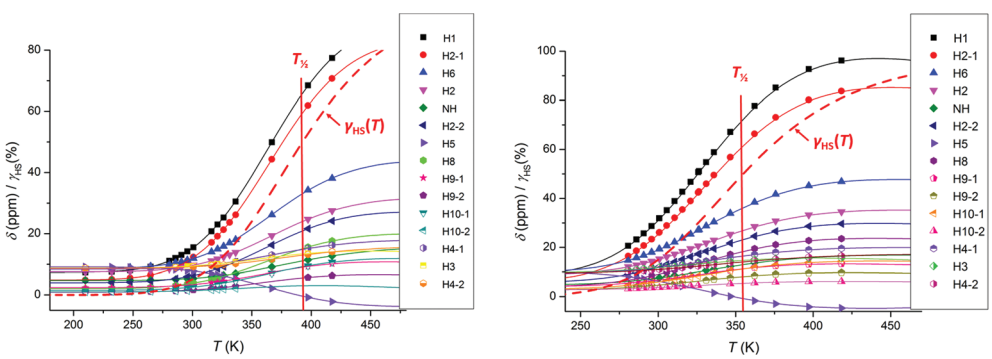

Fig. 2 Calculated (lines) *vs.* observed (symbols) chemical shifts for complex $[Fe^{2+}(rac\text{-}trans\text{-}5)]^{2+}$ in d_7-dmf (left) and d_5-nitrobenzene (right). The dashed red line gives the calculated HS fraction (%). The vertical axes have been used for the chemical shift (given in ppm) and HS fraction (given in %).

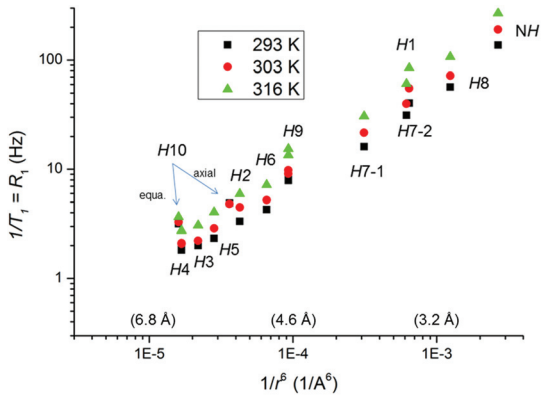

Fig. 3 Distance dependence of the longitudinal relaxation rates R_1 for [Fe(*rac*-*trans*-**5**)]$^{2+}$; *r* denotes the distance of a particular proton from the metal center. The logarithmic scale was used for sake of visual clarity.

between the HS and LS state (last term in eqn (11)[38]). This is corroborated by the large ratio of R_2/R_1 found for the protons with the largest Curie constants (H1, H7-1) and the strong field dependence of the linewidth, namely of these protons.

$$R_{2(\mathrm{obs})} = (1-\gamma_{\mathrm{HS}})R_{2(\mathrm{LS})} + \gamma_{\mathrm{HS}}R_{2(\mathrm{HS})} + (1-\gamma_{\mathrm{HS}})\gamma_{\mathrm{HS}}\frac{\Delta\omega^2}{k_{\mathrm{ex}}} \quad (11)$$

Qualitative description and calculation of kinetics

The first step in the calculation of the kinetics is the determination of the correlation time for the electron relaxation τ_s. This was achieved using the longitudinal relaxation rates and the distances between the protons and HS Fe^{2+} ion in [Fe(*rac*-*trans*-**5**)]$^{2+}$. The latter was approximated with respective Zn–H distances taken from the molecular structure of [Zn(*rac*-*trans*-**5**)]$^{2+}$, which serves as a structural model. Close structural agreement of iso-ligated complexes of Zn^{2+} and HS-Fe^{2+} had been previously found in many systems.[39,40] The correlation time for electron relaxation was calculated as τ_s = 1.1 ps (with $1/\tau_s$ = 900 GHz $\gg \omega_I$ = 3 GHz, as required). The correlation time for the electron relaxation also determines the ratio R_2/R_1 for the dipolar relaxation, which was calculated as R_2/R_1 = 1.1. With the calculated additional contribution of Curie relaxation to R_2, the expected ratio is R_2/R_1 = 1.46. With the known ratio R_2/R_1, the contribution of the exchange between HS and LS species to the linewidths can be isolated using eqn (11). The effect of *H*,*H*-coupling was corrected by subtraction.

We found that for protons H1 and H7-1, the linewidth is largely dominated by the exchange broadening. This observation can be ascribed to the large Curie constants (>30 000 ppm K with a large difference in the chemical shift between the HS and LS state) and, secondly, to the rather large distance of the proton site from the Fe^{2+} ion (>3.3 Å with large T_1). Both facts make these protons the best choice for further analysis (further useful sites are H6 and H2). The NH proton and H8 appear not to be suitable, being both close to the metal centre with large longitudinal relaxivity R_1 and a comparatively small Curie constant.

Based on H1, H2, H6 and H7-1, the time constant for the exchange between HS and LS state τ_{ex} ($1/\tau_{ex} = k_{HL} + k_{LH}$) was calculated to be 44 ns, 33 ns and about 28 ns at 293 K, 300.3 K and 316.1 K, respectively (Tables 12-SI to 14-SI†). To test the inner consistency of the calculations, the linewidth at 293 K for protons H1, H2, H6 and H7-1 as well as NH, H8, H5 and H7-2 at half the magnetic field was calculated and they agree well with experimentally obtained spectra (ESI Table 13-SI and Fig. 22-SI†).

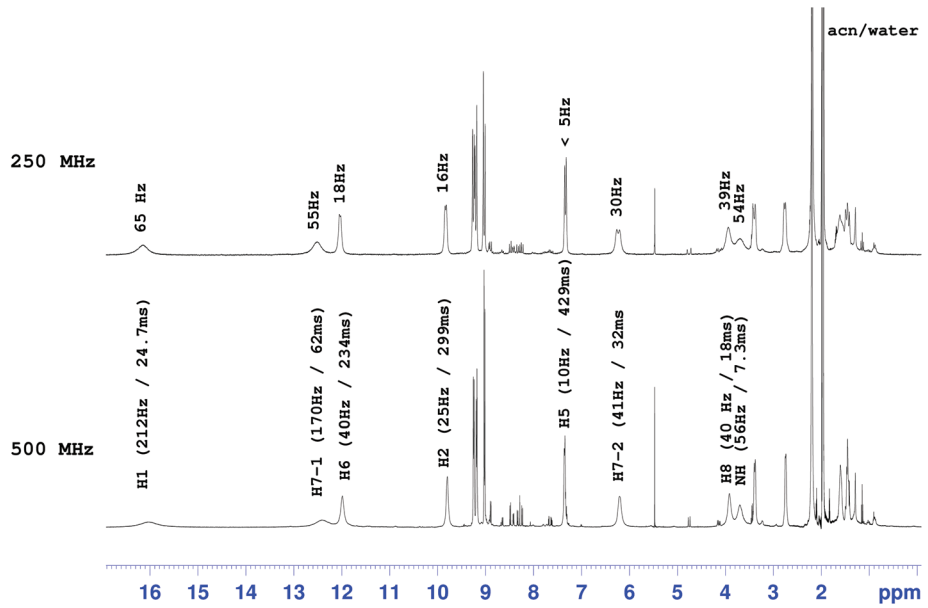

Fig. 4 ^{1}H NMR spectra of [Fe(*rac*-*trans*-**5**)]$^{2+}$ in d_3-acn solution recorded at 250 MHz and 500 MHz Larmor frequency. The assignment, linewidths (Hz), and T_1 times (at 500 MHz) are given. Note the strong field dependence for strongly shifted signals like H1 and H7-1.

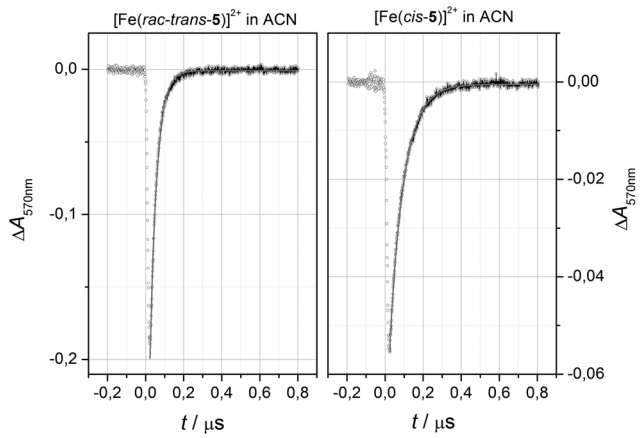

Fig. 5 Recovery profiles of transient absorption recorded at λ_{obs} = 570 nm after flashing (λ_{exc} = 532 nm) acetonitrile solutions at ambient temperature of [Fe(*rac-trans*-**5**)]$^{2+}$ (left) and [Fe(*cis*-**5**)]$^{2+}$ (right); symbols: experimental data; lines: mono-exponential fits. The exchange parameters for [Fe(*rac-trans*-**5**)]$^{2+}$ (left) and [Fe(*cis*-**5**)]$^{2+}$ (right) were fitted to τ_{ex} = 35.8(0.16) ns and τ_{ex} = 75.2(0.28) ns, respectively.

The NMR-derived results for the exchange kinetics (τ_{ex}) of [Fe(*rac-trans*-**5**)]$^{2+}$ were validated by laser flash photolysis (LFP) experiments in acn solution at ambient temperature. This method relies on light-induced population of the HS state *via* a rapid and selective relaxation cascade from the initially populated MLCT state. Decay of transient absorption directly reports on the kinetics of re-equilibration; mono-exponential fits to the experimental data provide reliable reference data for the relaxation kinetics of SCO compounds.[41–46]

Representative decay profiles obtained after excitation of the LS components of [Fe(*rac-trans*-**5**)]$^{2+}$ and [Fe(*cis*-**5**)]$^{2+}$ at λ_{exc} = 532 nm in dilute acn solution are shown in Fig. 5. The decay profiles have been recorded at the maximum wavelength of the intense MLCT transitions in the visible spectra range. The appearance as a bleach signal corresponds to the transient population of the spectroscopically transparent HS state. As required for uni-molecular reactions, the decay of the bleach signals is convincingly modeled by mono-exponential decay functions. The lifetimes of signal decay τ_{ex} are extracted from the fits. They closely agree with the NMR-derived values (τ_{ex}(^{1}H-NMR) = 33.7 ns *vs.* τ_{ex}(LFP/acn) = 35.8(0.16) ns). We take this compliance of methods as good evidence in favor of the herein applied NMR-based access to SCO kinetics. The individual reaction rates for the forward and backward reaction calculate to k_{HL} = 27.5 MHz and k_{LH} = 2.2 MHz, respectively. For sake of comparison, the relaxation rates of [Fe(*cis*-**5**)]$^{2+}$ are also extracted. We find them to be significantly longer (τ_{ex}(ACN) = 75.2(0.3) ns). This divergence reflects the lower thermodynamic driving force which is represented by the lower transition point $T_{1/2}$ of the latter compound.

Crystal structures

The molecular structures of complex dications [Zn(*rac-trans*-**5**)]$^{2+}$, [Fe(*rac-trans*-NMe-**5**)]$^{2+}$, [Fe(*cis*-**5**)]$^{2+}$ and [Fe(*rac-trans*-NMe-**6**)]$^{2+}$ were investigated by X-ray structure analysis in the solid state (Tables 16-SI and 167-SI†). All complexes are mononuclear with a distorted octahedral coordination sphere (Fig. 6 and 25-SI†). As expected the hexadentate ligands wrap around the Fe^{2+} ion with their two arms (one including N1–N2–N3 and the other N4–N5–N6). The two arms complement in a meridional arrangement similar to the situation in [Fe(terpy)$_2$]$^{2+}$ (terpy = 2,2′:6′,2″-terpyridine)[47–49] and related complexes.[7,9–11,13,14]

The secondary amines in [Zn(*rac-trans*-**5**)]$^{2+}$ and [Fe(*cis*-**5**)]$^{2+}$ form hydrogen bonds with the counter ions (BF_4^- and ClO_4^-). This finding supports the notion that hydrogen bonds are indeed responsible for the solvent dependence of $T_{\frac{1}{2}}$ observed for [Fe(*rac-trans*-**5**)]$^{2+}$. The diffraction data were collected at temperatures below 160 K. The high transition temperatures $T_{1/2}$ found in solution for the *trans*-complexes, transcribe into primarily LS character below room temperature. Accordingly, the Fe^{2+} ions in the crystal structures of [Fe(*rac-trans*-NMe-**5**)]$^{2+}$ and [Fe(**6**)]$^{2+}$ were found in the low spin state, as evidenced by the Fe–N bond lengths around 2.0 Å, both to the amine nitrogen atoms N1/N4 and to the terminal pyridine nitrogen atoms N3/N6. The Fe–N bond length to the inner pyridine rings, akin to [Fe(terpy)$_2$]$^{2+}$,[47–50] is even shorter (1.88 Å).

Bond lengths of the Fe^{2+} ion to the donating nitrogen atoms are much longer in [Fe(*cis*-**5**)]$^{2+}$ (2.23 Å to secondary amine and terminal pyridine nitrogens *versus* 2.1 Å to the inner pyridine) and are indicative of the HS state. The cyclohexyl ring of [Fe(*cis*-**5**)]$^{2+}$ is found in a preferred chair conformation. However, close intramolecular contact between two CH_2 units (C···C distance of 2.953 Å between C(H7)$_2$ and C(H9)$_2$) points to repulsions between the amino methylene group and the cyclohexyl ring that might destabilise the chair conformation and favor a twist boat conformer in the LS state. The activation energy of the transition of the chair conformer to the next stable twist boat conformer (20 kJ mol^{-1} above the chair conformation) is 44 kJ mol^{-1}.[51,52] This falls well within the available energy range to result in the observed irregular line broadening of this compound. A fast and complete ring flip at the NMR time scale would result in racemisation and in a pseudo C_2-symmetry in the NMR spectra; however no indication of higher symmetry was found in the NMR spectra.

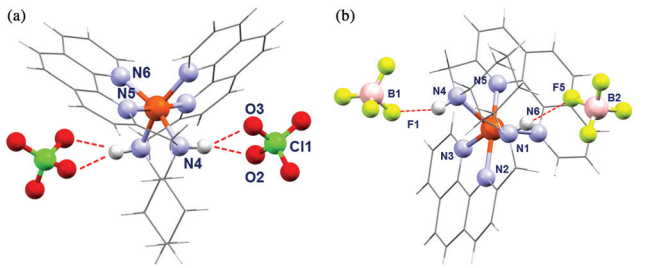

Fig. 6 Drawing of the molecular structure of (a) [Fe(*S*,*S*-**5**)]$^{2+}$ and adjacent ClO_4^- anions. Hydrogen bonds were found between O2···N4 (3.0266(1) Å) and O3···N4 (3.3864(1) Å). Note that the molecule has crystallographic C_2 symmetry and both ClO_4^--anions are equivalent by symmetry. (b) [Fe(*cis*-**5**)]$^{2+}$ and adjacent BF_4^--anions (hydrogen bonds are found between F5···N1 (2.81(3) Å) and F1···N4 (3.060(5) Å)).

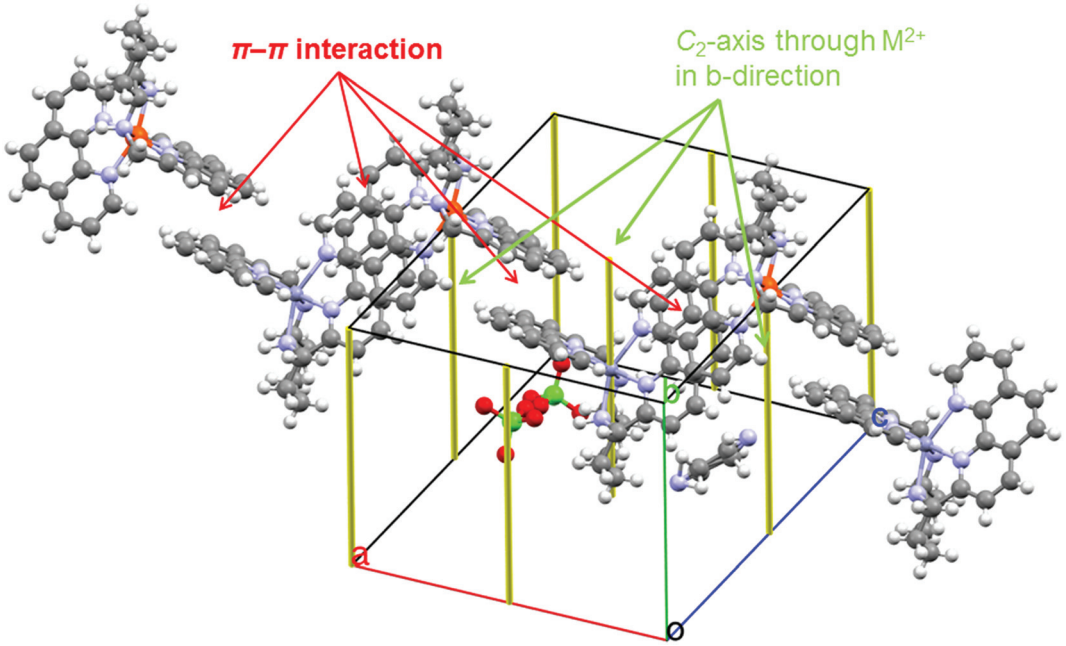

Fig. 7 Part of the crystal structure of [Zn(*R*,*R*-**5**)][Fe(*S*,*S*-**5**)](ClO$_4$)$_4$·(CH$_3$CN); both complex cations lie on crystallographic C_2-axes. In the direction of the *a*-axis, a chain with alternating Zn and Fe cations is formed by π,π stacking (colour scheme: Fe = orange, N = blue, Zn = gray).

Unfortunately any attempt to obtain [Fe(*rac-trans*-**5**)]X$_2$ as a single-crystal suitable for X-ray structure analysis failed. Irrespective of the chosen counter ions X$^-$, only microcrystalline samples were obtained. In contrast, the salt [Zn(*rac-trans*-**5**)](ClO$_4$)$_2$ crystallises in well-shaped crystals suitable for X-ray analysis. To obtain the molecular structure of [Fe(*rac-trans*-**5**)]$^{2+}$ (and to demonstrate its stability against ligand scrambling), we prepared the two enantiomerically pure complexes [Zn(*R*,*R*-**5**)](ClO$_4$)$_2$ and [Fe(*S*,*S*-**5**)](ClO$_4$)$_2$ starting from commercially available enantiomerically pure diamines *R*,*R-trans*-**4** and *S*,*S-trans*-**4**. Both complexes were combined as a 1 : 1 mixture in acetonitrile. To our delight, slow diffusion of ether vapors to this solution yielded crystals suitable for single crystal structure analysis.

Refinement in I_2 leads to two symmetry independent cations [M(*R*,*R-trans*-**5**)]$^{2+}$ and [M(*S*,*S-trans*-**5**)] with clearly different M–N bond lengths. One set of bond lengths is typical of LS Fe^{2+} while the other is typical of Zn^{2+}, allowing a preliminary assignment. In agreement with this assignment, the chiral configurations of the molecules matched the configurations of the starting materials and verified the quasi racemic crystal structure.[12] To verify the results, ESI mass spectra were recorded using the original crystal that had been used for data collection. Indeed, both cations were found in a 1 : 1 ratio with the expected isotopic pattern (Fig. 26-SI†), thus corroborating the assignment of the crystal composition as [Zn(*R*,*R*-**5**)][Fe(*S*,*S*-**5**)](ClO$_4$)$_4$·(CH$_3$CN). In the crystal structure, the [Zn(*R*,*R*-**5**)]$^{2+}$ cations and [Fe(*S*,*S*-**5**)]$^{2+}$ cations are threaded along different C_2 axis with an opposite sense of direction. As a consequence, both cations have crystallographic induced C_2 symmetry. Between the phenanthroline groups of the Zn and Fe complex cations π–π contacts (3.3 Å plane distance) were found, forming a chain with alternation of Fe and Zn cations along the direction of the *a*-axis (Fig. 7).

Electrochemistry

The previous discussion of the ^{1}H NMR and UV/Vis spectra pointed out effects of *N*-methylation of the ligand-appended *N*H groups on the thermodynamics of SCO. Cyclic voltammetry was used to track concomitant effects on the redox chemistry (Table 18-SI and Fig. 28-SI†). All complexes under study show reversible or quasi-reversible oxidation processes. Exceptionally, the redox wave of [Fe(*rac-trans*-NMe-**6**)]$^{2+/3+}$ has a large peak separation of 103 mV. The large peak separation likely occurs for the same reason as previously given for the unusual NMR broadening; we think that the redox event includes two redox couples with slightly different redox potentials for two different conformations of the cyclohexyl ring. An alternative interpretation in terms of SCO appears unlikely, because for Fe^{2+} SCO complexes usually only one well reversible redox process is found due to the fast spin equilibrium.[53]

A substantial effect of *N*-methylation on the metrics of both, SCO and redox, became evident in previous work on a structurally related complex, employing a 2,2′-diamino-1,1′-biphenyl bridge.[9] For instance, in this latter case, the methylation of the secondary amine resulted in a dramatic shift of the spin-state energies. Thermal SCO behavior applied to the non-*N*-methylated complex ($T_{\frac{1}{2}}$ = 403 K), whereas purely HS character arises for the *N*-methylated complex. At the same time, the oxidation potential for the Fe$^{2+/3+}$ redox transition shifted by 300 mV to more anodic potentials.[9] Both effects were ascribed to steric reasons; that is, to the repulsion between the methyl

groups and the biphenyl core that hinders the approach of the ligand to the metal center and therefore favors the HS state or the $Fe^{2+/3+}$-ion with the larger ion diameter.

Also in the present case the *N*-methylation has a significant impact on the redox potentials. Correspondingly, the complexes investigated in this study can be grouped into two categories along the status of substitution of the amine groups: accordingly and in agreement with previous experience, non-*N*-methylated complexes ($E^{0'}$ = 465 mV ([Fe(*rac-trans*-**5**)]$^{2+/3+}$); $E^{0'}$ = 487 mV ([Fe(*cis*-**5**)]$^{2+/3+}$)) are more susceptible towards oxidation than their *N*-methylated congeners ($E^{0'}$ = 570 mV [Fe(*rac-trans*-NMe-**5**)]$^{2+/3+}$ and $E^{0'}$ = 540 mV [Fe(*rac-trans*-NMe-**6**)]$^{2+/3+}$). Akin to the aforementioned 2,2′-diamino-1,1′-biphenyl bridged complexes, *N*-methylation causes an anodic shift of the redox potentials, admittedly by only 100 mV. However, here the stabilization of the Fe^{2+}-redox state by *N*-methylation is accompanied by an inverted effect on $T_{\frac{1}{2}}$. That is, for the two redox pairs [Fe(*rac-trans*-**5**)]$^{2+/3+}$ and [Fe(*rac-trans*-NMe-**5**)]$^{2+/3+}$, the methylation stabilises the LS state.

On first glance this seems contradictory; the *N*-methylated tertiary amine is a better donor than the secondary amine and should support the higher oxidation state, but an opposite effect is observed. Likely, the reason is the increased shielding of the metal center by the methyl groups. Charges are usually screened by a surrounding solvent cage. The dipole moments of the oriented solvent molecules are preferentially aligned in an opposite direction with the electric field and reduce the effective charge on the metal complex. The non-methylated complexes [Fe(*rac-trans*-**5**)]$^{2+/3+}$ and [Fe(*cis*-**5**)]$^{2+/3+}$ can form hydrogen bonds that support the alignment of solvent (acn) dipole moments opposite to the electric field and therefore increase the charge compensating effect of the solvent cage. This effect facilitates the oxidation of non-*N*-methylated complexes and stabilises the *N*-methylated complexes in the Fe^{2+} oxidation state. Obviously this effect is larger than the electron donating effect of the additional methyl groups [Fe(*rac-trans*-NMe-**5**)]$^{2+/3+}$. This line of argumentation is in agreement with the outcomes of the solvatochromism studies (see the ESI†).

Conclusion

In conclusion, we have prepared a series of Fe^{2+} SCO complexes employing hexadentate ligands with 1,2-diaminocyclohexanes (**4**) as central building blocks. The chelating effect and the rigid structure of the ligand make the complexes exceptionally robust. They are inert even against coordinating solvents like dmso at high temperatures. We investigated their solution behaviour by using VT ^{1}H NMR spectroscopy and VT Vis spectroscopy. For the first time we have demonstrated that by using VT ^{1}H NMR spectroscopy the thermodynamics as well as kinetics for SCO can be obtained. VT ^{1}H NMR spectroscopy has the major advantages of being a species-specific, non-bulk method offering the high precision of a few Hz in a range of about 50 000 Hz. The complex investigated in this survey, namely [Fe(*rac-trans*-**5**)]$^{2+}$, shows a comparatively fast SCO with correlation time in the 10 ns-timescale. With increasing correlation time for SCO ($\tau_{sco} = 1/k_{ex}$), the ratio between exchange broadening and paramagnetic relaxation becomes more convenient for the analysis and allows instantaneous identification of slow SCO processes in Fe^{2+}–SCO-complexes.[41,54] Moreover, use of very high field magnets (>600 MHz) will shorten the timescale further allowing elucidation of SCO kinetics down to the 1 ns-timescale. The solvent dependence of $T_{1/2}$ found for complex [Fe(*rac-trans*-**5**)]$^{2+}$ is ascribed to hydrogen bond formation of the secondary amine and the solvent. The cyclic voltammetry experiments also revealed the dominant effect of the hydrogen bonds to the secondary amine on the redox potentials. Enantiomeric pure complexes can be prepared starting with *R*,*R*- or *S*,*S*-1,2-diaminocyclohexane (*R*,*R*-*trans*-**4** or *S*,*S*-*trans*-**4**). The high robustness of the complexes reduces a possible ligand scrambling and allows preparation of quasiracemic crystals of [Zn(*R*,*R*-**5**)][Fe(*S*,*S*-**5**)]$(ClO_4)_4\cdot(CH_3CN)$ including a 1 : 1 mixture of the Zn and Fe complexes with inverse chirality. Furthermore we demonstrated the incorporation of the complexes [Fe(*rac-trans*-**5**)]$^{2+}$ and [Fe(*rac-trans*-NMe-**5**)] in epoxy resins by dissolving an appropriate salt in the hardener before mixing with the resin.

Experimental

Experimental details for the synthesis and characterisation of the materials, details on the crystal structure refinement and a detailed description of the methods used are compiled in the ESI.† The results of the crystal structure analysis for compounds [Fe(*cis*-**5**)]$(BF_4)_2\cdot(0.5\cdot CH_3CN)$ (CCDC 1472618), [Fe(*rac-trans*-NMe-**5**)]$(BF_4)_2\cdot(0.5\cdot CH_3CN)$ (1472619), [Zn(*rac-trans*-**5**)]$(ClO_4)_2\cdot(CH_3CN)$ (1472620), [Zn(*R*,*R*-**5**)][Fe(*S*,*S*-**5**)]$(ClO_4)_4\cdot 2(CH_3CN)$ (1472621) and [Fe(*rac-trans*-NMe-**6**)]$(BF_4)_2$ (1472622) were deposited in the CSD data base.

Acknowledgements

This work was financially supported by the DAAD, Fonds der Chemischen Industrie (Liebig Stipendium) and the Deutsche Forschungsgemeinschaft DFG (PE1513/4-1). G. H. thanks Dr Tomasz Pedzinski (AMU Poznan) for assistance with laser-flash photolysis. G. H. acknowledges support of this work by the Deutsche Forschungsgemeinschaft(SFB 658, Elementary processes in molecular switches on surfaces).

Notes and references

1 M. A. Halcrow, *Structure: Function Relationships in Molecular Spin-Crossover Materials*, Wiley & Sons, Chichester, 2013.
2 P. Gütlich, Y. Garcia, H. A. Goodwin, Y. Garcia and H. A. Goodwin, *Chem. Soc. Rev.*, 2000, **29**, 419–427.
3 P. Gütlich and A. Hauser, *Coord. Chem. Rev.*, 1990, **97**, 1–22.
4 H. Toftlund, *Coord. Chem. Rev.*, 1989, **94**, 67–108.

5 P. Gütlich, A. B. Gaspar and Y. Garcia, *Beilstein J. Org. Chem.*, 2013, **9**, 342–391.
6 P. Gütlich, A. Hauser and H. Spiering, *Angew. Chem., Int. Ed.*, 1994, **106**, 2109–2141.
7 H. Petzold and S. Heider, *Eur. J. Inorg. Chem.*, 2011, 1249–1254.
8 S. Heider, H. Petzold, G. Chastanet, S. Schlamp, T. Rüffer, B. Weber and J.-F. Létard, *Dalton Trans.*, 2013, **42**, 8575–8584.
9 S. Heider, H. Petzold, J. M. Speck, T. Rüffer and D. Schaarschmidt, *Z. Anorg. Allg. Chem.*, 2014, **640**, 1360–1367.
10 S. Heider, H. Petzold and G. Teucher, *Eur. J. Inorg. Chem.*, 2013, **2013**, 2382–2388.
11 E. C. Constable, G. Zhang, C. E. Housecroft, M. Neuburger and J. A. Zampese, *Eur. J. Inorg. Chem.*, 2010, 2000–2011.
12 Y. Popowski, I. Goldberg and M. Kol, *Chem. – Eur. J.*, 2016, **22**, 5530–5533.
13 N. A. Hall, C. Duboc, M.-N. Collomb, A. Deronzier and A. G. Blackman, *Dalton Trans.*, 2011, **40**, 12075–12082.
14 L. J. Baird, C. A. Black and A. J. Blackman, *Polyhedron*, 2007, **26**, 378–384.
15 M. P. Shores, C. M. Klug and S. R. Fiedler, in *Spin-Crossover Mater*, ed. M. A. Halcrow, Wiley & Sons, 2013, pp. 281–301.
16 P. Pallavicini, V. Amendola, Y. D. Fernandez, M. Ghisalberti, L. Linati, C. Mangano, A. M. Lanfredi and C. Massera, *Dalton Trans.*, 2003, 575–580.
17 V. Hebbe-Viton, V. Desvergnes, J. J. Jodry, C. Dietrich-Buchecker, J.-P. Sauvage and J. Lacour, *Dalton Trans.*, 2006, 2058–2065.
18 G. J. P. Britovsek, J. England and A. J. P. White, *Dalton Trans.*, 2006, 1399–1408.
19 A. Borgogno, F. Rastrelli and A. Bagno, *Dalton Trans.*, 2014, **43**, 9486.
20 G. P. I. Bertini and C. Luchinat, *Solution NMR of Paramagnetic Molecules*, Elsevier, 2001.
21 J. P. Jesson, S. Trofimenko and D. R. Eaton, *J. Am. Chem. Soc.*, 1967, **89**, 3158–3164.
22 K. Bryliakov, E. Duban and E. Talsi, *Eur. J. Inorg. Chem.*, 2005, 72–76.
23 S. E. Creutz and J. C. Peters, *Inorg. Chem.*, 2016, **55**, 3894–3906.
24 S. A. Barrett, C. A. Kilner and M. A. Halcrow, *Dalton Trans.*, 2011, **40**, 12021–12024.
25 B. Strauß, V. Gutmann, W. Linert and B. Strauß, *Monatsh. Chem.*, 1993, **124**, 515–522.
26 Z. Ni, A. M. McDaniel and M. P. Shores, *Chem. Sci.*, 2010, **1**, 615.
27 Z. Ni and M. P. Shores, *J. Am. Chem. Soc.*, 2009, **131**, 32–33.
28 Z. Ni and M. P. Shores, *Inorg. Chem.*, 2010, **49**, 10727–10735.
29 B. Weber, W. Bauer, T. Pfaffeneder, M. M. Dîrtu, A. D. Naik, A. Rotaru and Y. Garcia, *Eur. J. Inorg. Chem.*, 2011, **2011**, 3193–3206.
30 B. Weber, E. S. Kaps, J. Obel, K. Achterhold and F. G. Parak, *Inorg. Chem.*, 2008, **47**, 10779–10787.
31 B. Weber, W. Bauer and J. Obel, *Angew. Chem.*, 2008, **120**, 10252–10255.
32 B. Weber and F. A. Walker, *Inorg. Chem.*, 2007, **46**, 6794–6803.
33 P. Basu, N. V. Shokhirev, J. H. Enemark and F. A. Walker, *J. Am. Chem. Soc.*, 1995, **117**, 9042–9055.
34 F. A. Walker, *Inorg. Chem.*, 2003, **42**, 4526–4544.
35 B. Weber, J. Obel, D. Henner-Vasquez and W. Bauer, *Eur. J. Inorg. Chem.*, 2009, 5527–5534.
36 B. Weber, C. Carbonera, C. Desplances and J.-F. Letard, *Eur. J. Inorg. Chem.*, 2008, 1589–1598.
37 Z. Xia, B. D. Nguyen and G. N. La Mar, *J. Biomol. NMR*, 2000, **17**, 167–174.
38 J. S. Leigh, *J. Magn. Reson.*, 1971, **311**, 308–311.
39 N. Paradis, G. Chastanet, F. Varret and J. Létard, *Eur. J. Inorg. Chem.*, 2013, **2013**, 968–974.
40 P. Chakraborty, C. Enachescu, C. Walder, R. Bronisz and A. Hauser, *Inorg. Chem.*, 2012, **51**, 9714–9722.
41 P. Stock, T. Pędziński, N. Spintig, A. Grohmann and G. Hörner, *Chem. – Eur. J.*, 2013, **19**, 839–842.
42 S. Schenker, P. C. Stein, J. A. Wolny, C. Brady, J. J. Mcgarvey, H. Toftlund and A. Hauser, *Inorg. Chem.*, 2001, **40**, 134–139.
43 J. J. McGarvey, H. Toftlund, A. H. R. Al-Obaidi, K. P. Taylor and S. E. J. Bell, *Inorg. Chem.*, 1993, **32**, 2469–2472.
44 A. H. R. Al-Obaidi, K. B. Jensen, J. J. McGarvey, H. Toftlund, B. Jensen, S. E. J. Bell and J. G. Carroll, *Inorg. Chem.*, 1996, **35**, 5055–5060.
45 P. Stock, E. Deck, S. Hohnstein, J. Korzekwa, K. Meyer, F. W. Heinemann, F. Breher and G. Hörner, *Inorg. Chem.*, 2016, **55**, 5254–5265.
46 P. Stock, N. Spintig, J. Scholz, J. D. Epping, C. Oelsner, D. Wiedemann, A. Grohmann and G. Hörner, *J. Coord. Chem.*, 2015, **68**, 3099–3115.
47 A. Hauser, C. Enachescu, M. L. Daku, A. Vargas and N. Amstutz, *Coord. Chem. Rev.*, 2006, **250**, 1642–1652.
48 F. Pelascini, M. Wesolek, F. Peruch, A. De Cian, N. Kyritsakas, P. J. Lutz and J. Kress, *Polyhedron*, 2004, **23**, 3193–3199.
49 G. U. Priimov, P. Moore, P. K. Maritim, P. K. Butalanyi and N. W. Alcock, *J. Chem. Soc., Dalton Trans.*, 2000, **1**, 445–449.
50 L. J. K. Cook, F. Tuna and M. A. Halcrow, *Dalton Trans.*, 2013, **42**, 2254–2265.
51 D. Bucher, L. C. T. Pierce, J. A. McCammon and P. R. L. Markwick, *J. Chem. Theory Comput.*, 2011, **7**, 890–897.
52 G. Gill, D. M. Pawar and E. A. Noe, *J. Org. Chem.*, 2005, 10726–10731.
53 J. W. Turner and F. A. Schultz, *Coord. Chem. Rev.*, 2001, **219–221**, 81–97.
54 E. C. Constable, G. Baum, E. Bill, R. Dyson, R. V. Eldik, D. Fenske, S. Kaderli, D. Morris, A. Neubrand, M. Neuburger, *et al.*, *Chem. – Eur. J.*, 1999, **5**, 498–508.